Inorganica Chimica Acta 464 (2017) 99–107

Contents lists available at ScienceDirect

Inorganica Chimica Acta

journal homepage: www.elsevier.com/locate/ica

Research paper

Synthesis of polyethylene and PE/MWCNT composite using a spherical bulky α-diimine Pd(II) catalyst

Mahsa Kimiaghalam [a], Hossein Nasr Isfahani [a], Gholamhossein Zohuri [b,*], Ali Keivanloo [a]

[a] Department of Chemistry, Shahrood University of Technology, Shahrood, PO Box 3619995161, Iran
[b] Department of Chemistry, Faculty of Sciences, Ferdowsi University of Mashhad, Mashhad, PO Box 91775, Iran

ARTICLE INFO

Article history:
Received 26 March 2017
Received in revised form 30 April 2017
Accepted 3 May 2017
Available online 5 May 2017

Keywords:
Catalytic polymerization
Polyethylene
α-diimine palladium catalyst
Benzhydryl
Nanocomposite

ABSTRACT

The ligand N,N-bis(2,6-dibenzhydryl-4-ethoxy phenyl)butane-2,3-diimine via a multi-step reaction and the correspond palladium(II) α-diimine catalyst were synthesized, characterized and used in polymerization of ethylene. The effects of polymerization condition were investigated which the α-diimine catalyst was active up to 80 °C. The highest activity of the catalyst (330 kg of PE (mol Pd^{-1} h^{-1}) was obtained at 2 equivalent NaBAF (cocatalyst), T_p = 40 °C and P_{Et} = 5 bar. GPC analysis revealed that the $\overline{Mw}$ of polyethylene virtually was equal to 8.1×10^4 g/mol along with PDI = 1.83. The structure of complex was optimized and the theoretical parameters were presented. The synthesized PE/MWCNT nanocomposite via in-situ polymerization showed the higher thermal stability (27 °C in presence of 3.88% MWCNT) than neat PE. Investigation of samples morphology by SEM, showed the morphology of the catalyst and PE were virtually spherical according to replication phenomenon and the MWCNTs acted as a bridge and end-cap in the polymer matrix.

1. Introduction

Over the past few decades enormous research has been conducted on single-site olefin polymerization catalysts [1]. In the field of α-diimine catalysts significant advances have been made through modification of the ligand backbone and the *N*-aryl substituent [2,3]. The ortho substituents retard chain transfer reactions, promote the chain walking and accelerate the rate of migratory insertion. So steric bulkiness of the ortho substituents have influence on the molecular weight and branching density of polyethylene and catalyst activities [4]. The thermal stability of catalyst were improved by using bulky substituents[5]. Recently, benzhydryl-derived ligand frameworks were investigated [6–10]. The size, nature and regiochemistry of the substituents in the iminoaryl groups have crucial importance in controlling the polymerization and oligomerization [11–14]. The branching density of polymers is a significant factor that affects the polymer physical properties. Also other factors like relative rate of ethylene insertion and chain walking change these properties. Chen et al. showed that the polymer molecular weight, branching density and the distribution of short-chain branches are relatively independent of polymerization conditions and just modification of the α-diimine ligands in Pd(II) systems control the polymer properties [15].

Recently, Chen et al. demonstrated the synthesis of polyethylene (PE) with very low branching densities (23–29/1000C) using some α-diimine Pd(II) complexes bearing a dibenzhydryl moiety and different *N*-aryl substituent in para position (Me, OMe, Cl, CF_3) [8]. Herein, we synthesized and characterized a α-diimine Pd(II) complex with benzhydryl-derived ligand framework and ethoxy group in the para position of *N*-aryl groups as catalyst structure shown in Fig. 1. The electronic effects of the ligand controlled by ethoxy group as an electron-donating group. The ligand electronic effects upon the catalytic activity in different polymerization condition, thermal stability of the complex and polymer properties were investigated. In addition to synthesis of new catalyst structures, there are a huge trend in introducing components such as nanomaterials to the polymerization systems which can modify or enhance the catalyst behavior and polymer properties [16–22]. Carbon nanotubes are promising fillers for composite materials to improve polymer properties. Some common methods for the preparation of polymer/CNT composites include in situ polymerization [23,24], solution mixing [25–27], and melt blending [28–30].

In this research, we also investigated the effect of multi-walled carbon nanotubes (MWCNT) on the catalyst behavior and

* Corresponding author.
E-mail address: zohuri@um.ac.ir (G. Zohuri).

http://dx.doi.org/10.1016/j.ica.2017.05.005
0020-1693/

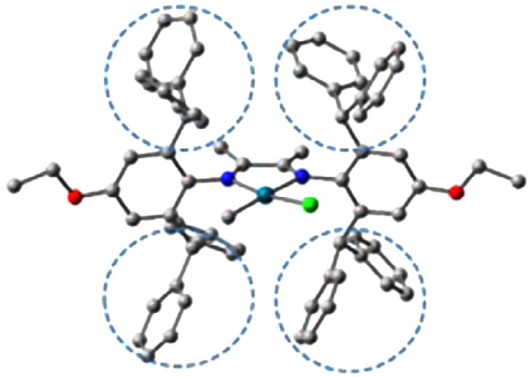

Fig. 1. Optimized structure of the Pd catalyst complex, Hydrogen atoms omitted to simplify.

properties of the polyethylene which the polymerization of ethylene in presence of the catalyst occurred directly on the MWCNTs surface [31].

2. Experimental

2.1. Materials

All manipulation of air and water-sensitive compounds were conducted under inert atmosphere (N_2/Ar) using standard Schlenk and glove box techniques. Argon, nitrogen and ethylene gas were purified by passing through activated columns of silica gel, KOH and 4Å molecular sieve. All the solvents were dried prior to use. Toluene was dried over calcium hydride and distilled over sodium/benzophenone. Dichloromethane and *n*-hexane also were purified over calcium hydride and the diethyl ether was purified over sodium/benzophenone. 4-Ethoxy aniline (purity 99.9%) (Merck) was distilled. Diacetyl (97%), diphenyl methanol (98%) were supplied by Merck Chemicals. Chloro (1,5-cyclooctadiene) methyl palladium and sodium tetrakis (3,5-bis (trifluoromethyl) phenyl borate were purchased from sigma Aldrich chemicals. $MWCNT_{20-30\ nm}$ (95%) and $MWCNT_{30-50\ nm}$ (95%) were purchased from US research nanomaterials.

2.2. Instrumentation

^{1}H and ^{13}CNMR spectra for organic compounds were recorded at Bruker-Avance III (300 MHz). High temperature NMR analysis of polyethylene was performed on a Bruker-Avance 400 (400 MHz). Elemental analysis was performed by Thermi finnigan EA1112 CHN elemental analyzer. FT-IR spectra were obtained using Avatar 370 FT-IR spectrometer. Mass spectrum were recorded using Varian CH-7A spectrometer. Thermal gravimetric analysis (TGA) (Perkin Elmer TGA-7) and differential scanning calorimetry (DSC) Mettler Toledo DSC 822^e with a rate of 10 °C/min were used for characterization of polyethylene and nanocomposites samples. Scanning electron microscope (SEM) images were obtained using LEO VP 1450 Instrument. High temperature Gel permeation chromatography (GPC) was performed in 3-chloro benzene solvent (PL-GPC 220).

2.3. The synthesis of ligand

The synthesis of N,N′-bis(2,6-dibenzhydryl-4-ethoxy phenyl) butane-2,3-diimine was completed in two steps from commercially available starting materials.

2.3.1. Synthesis of 2,6-Bis(diphenyl)-4-ethoxyaniline

2,6-Bis(diphenylmethyl)ethoxy-aniline was synthesized according to the literature [8] which in a 250 ml round-bottom flask was charged with para ethoxy aniline (2.57 ml, 20.0 mmol) and diphenylmethanol (7.36 g, 40 mmol), the mixture was heated to 120 °C. A solution of anhydrous zinc chloride (0.681 g, 5 mmol) in concentrated hydrochloric acid (37% in H_2o) was added to the mixture (exothermic) and the temperature was raised to 160 °C. After 30 min at 160 °C, the reaction mixture was allowed to cool down and dissolved in CH_2Cl_2 (200 ml). The CH_2Cl_2 layer was washed out with water (3 × 100 ml) and dried over anhydrous sodium sulfate. The solution was concentrated to 20 ml and the product was crash out with 200 ml methanol. The pure desired aniline was obtained as a white crystalline solid by recrystallization. mp: 191 °C, ^{1}HNMR (300 MHz, $CDCl_3$, δ, ppm): 7.04–7.26 (m, 20H, aryl-H), 6.16 (S, 2H, aryl-H), 5.44 (S, 2H, $CHPh_2$), 3.52–3.59 (q, 2H, OCH_2), 3.08 (S,2H,NH_2), 1.11–1.16 (t, 3H, CH_3), ^{13}C NMR (300 MHz, $CDCl_3$, δ, ppm): 151.19 (O—$C^{P\text{-}Ar}$), 142.57, 135.83, 130.81, 129.54, 128.54, 126.70, 115.06, 63.30 ($CHPh_2$), 52.49 (O—CH_2), 14.79 (CH_3). MS (*m*/*z*); calcd for $C_{34}H_{31}NO$, 469.62; found, 471[M+H]$^+$. Anal. Calcd: C, 86.96; H, 6.65; N, 2.98. Found: C, 85.67; H, 6.37; N, 2.86. IR cm^{-1} (KBr); 3427.4, 3363.93 (NH_2), 1263.52 (C—O).

2.3.2. The synthesis of N,N′-bis(2,6-dibenzhydryl-4-ethoxy phenyl) butane-2,3-diimine

A solution of prepared aniline in previous section (1.4 g, 2.98 mmol), 2,3-butadione (0.129 ml, 1.49 mmol), and p-toluene sulfonic acid (20 mg, 0.116 mmol) in toluene (200 ml) was stirred at 80 °C for 24 h, then the reaction was refluxed with Dean-stark trap for 4 days. The solvent was evaporated and the remaining solution was diluted in methanol (125 ml). The yellow solid was isolated by filtration, washed several times by 20 ml methanol and dried under high vacuum. The pure desired product was obtained as a yellow crystalline solid by recrystallization. mp: 242 °C.

^{1}HNMR (300 MHz, $CDCl_3$, δ, ppm): 7.24–7.14 (m, 24H, aryl-H), 7.04(d, 8H, aryl-H), 6.96 (d, 8H,aryl-H), 6.42 (s, 4H, aryl-H), 5.15 (s, 4H, $CHPh_2$), 3.68–3.74 (q, 4H, OCH_2), 1.21–1.25 (t, 6H, CH_3), 1.15 (s, 6H, N=C—Me), ^{13}CNMR (300 MHz, $CDCl_3$, δ, ppm): 170.51 (N=C—Me), 154.52 (O—$C^{P\text{-}Ar}$), 143.50, 142.74, 141.57, 132.23, 129.64, 129.38, 128.39, 128.10, 126.43, 126.15, 114.60, 63.26 (O—CH_2), 51.76 ($CHPh_2$), 16.65 (N=C-Me), 14.75 (CH_3). IR (KBr, cm^{-1}); 1262 (C—N), 1639.17 (C=N). Anal. calcd for $C_{72}H_{64}N_2O_2$: C, 87.41; H, 6.52; N, 2.83. Found: C, 87.98; H, 6.19; N, 2.82.

2.4. Synthesis of methyl chloride palladium complex

To a solution of prepared ligand (0.17 g, 0.171 mmol) in dry CH_2Cl_2 (5 ml), Pd(COD)MeCl (0.045 g, 0.171 mmol) was added. After stirring the mixture for 3 days at room temperature, the solvent was partially evaporated under reduced pressure and the remaining solution was diluted in diethyl ether. The orange solid was isolated by centrifuge and dried under high vacuum. This pre-catalyst was used in polymerization process without further purification. ^{1}HNMR (300 MHz, $CDCl_3$, δ, ppm): 7.45 (d, 4H, aryl-H), 7.34 (d, 4H, aryl-H), 7.20–7.01 (m, 32H, aryl-H), 6.71 (S, 2H, aryl-H), 6.48 (S, 2H, aryl-H), 5.96 (S, 2H, $CHPh_2$), 5.71 (S, 2H, $CHPh_2$), 3.83–3.76 (q, 2H, OCH_2), 3.73–3.66 (q, 2H, OCH_2), 1.23–1.22 (t, 3H, CH_3), 1.20–1.09(t, 3H, CH_3), 0.65 (S, 3H, Pd—Me), 0.34 (S, 3H, N=C—Me), 0.12 (S, 3H, N=C—Me). Anal. calcd for $C_{73}H_{67}ClN_2O_2Pd$: C, 76.49; H, 5.89; N, 2.44; Found: C, 75.77; H 5.62; N, 2.25; IR (KBr, cm^{-1}); 1577.90 (C=N), 528.7(Pd—C), 437.73 (Pd—N).

2.5. General procedure for catalyzed ethylene polymerization

The low pressure polymerization process was carried out in two-neck flask which was equipped with magnetic stirrer and ethylene inlet. While, the high pressure process was performed in a 1-L Buchi bmd 300-type stainless steel reactor. Prior to each polymerization reaction, the reactor was purged with argon gas at 120 °C for about 1 h to ensure the absence of any moisture and oxygen.

The synthesis of PE/MWCNT composites were carried out through the in-situ polymerization method. A mixture of desired amount of MWCNT and catalyst were introduced into the reactor in presence of co-catalyst under ethylene atmosphere.

3. Results and discussion

3.1. Synthesis of ligand and palladium complex

Steps as shown in Scheme 1. acid catalyzed reaction of diphenyl methanol with distilled para ethoxy aniline in a 2:1 mol ratio gave 2,6-bis(diphenyl methyl)-4-ethoxyaniline, which was further reacted with di-acetyl via *p*-toluene sulfonic acid catalyzed reaction to obtain yellow α-diimine ligand. All spectral data for prepared compounds are given in section 2. Aromatic protons in ^{1}HNMR spectrum of ligand appears in 6.16–7.04 ppm, this shielding is due to ethoxy groups effect. Also the absence of carbonyl carbon and the presence of imine carbons in the ^{13}CNMR and IR spectra of ligand supported successful synthesis of desired ligand and also number of peaks in ^{1}HNMR and ^{13}CNMR confirm symmetrical ligand structure. (α-diimine) palladium (II) catalyst was obtained by reacting the α-diimine ligand with (COD)PdMeCl in dichloromethane at room temperature. The process illustrated in Scheme 2. Stable palladium complex was formed in dichloromethane solvent via displacement of 1,5-cyclooctadiene(COD) from (COD)PdMeCl by 1 equivalent of α-diimine ligand. Crystalline complex could be obtained at room temperature by diffusion of diethylether or *n*-Hexane into dichloromethane solution of the corresponding complex. The structure of the product was deduced from its elemental analysis and IR, ^{1}H NMR spectral data. The ^{1}HNMR spectrum of complex confirm asymmetrical and rigid structure. ^{1}H NMR spectroscopy indicated the generation of other product as a impurities that was not identified, but may correspond to the complexation of the ligand to Pd(II) through one imine nitrogen atom.

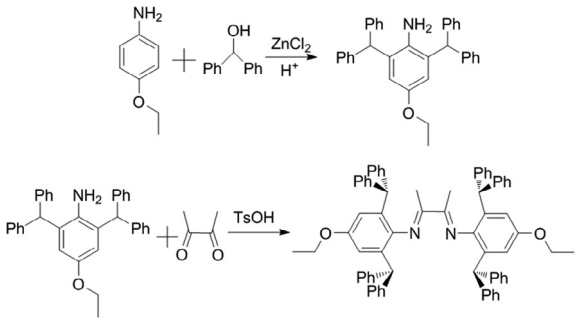

Scheme 1. Synthesis route of ligand.

3.2. Ethylene polymerization

The results of ethylene polymerization catalyzed by prepared catalyst are listed in Table 1. The ethylene polymerization was carried out in different conditions. A direct in situ activation procedure was employed which the palladium complex was treated with sodium tetrakis (3,5-bis(trifluoromethyl phenyl) borate (NaBAF) to yield the cationic palladium complex. The polymerization activity increased with addition of co-catalyst up to 2 equivalent. The effect of temperature on the catalyst behavior was investigated in the range of 25° to 80 °C at constant 1.5 bar of ethylene pressure. The prepared catalyst showed high thermal stability. It reached its highest activity at 40 °C and maintained activity even at 80 °C. Study on polymerization temperature and kinetic of polymerization on the catalyst behavior revealed that polymerization temperature can enhance the catalyst performance through increasing the kinetic energy of the monomer molecules which facilitates transfer of ethylene to the catalytic active centers and increasing alkylation of metal centers up [32].

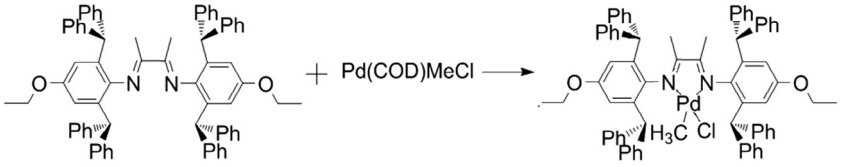

Scheme 2. Synthesis route of catalyst.

Table 1
Ethylene polymerization and nano composite synthesis results using Pd/NaBAF system.

Entry	CoCat. (eq)	T (C)	P (atm)	Activity	CNT (mg)	$M_v(10^4)$	$M_n(10^4)$	$M_w(10^4)$	Branch/1000C
1	1.2	40	1.5	111	–	–	–	–	–
2	1.5	40	1.5	116	–	–	–	–	–
3	2.0	40	1.5	168	–	6.75	4.40	**8.09**	**40.5**
4	2.0	25	1.5	92	–	4.59	–	–	–
5	2.0	60	1.5	131	–	5.46	–	–	–
6	2.0	80	1.5	67	–	1.73	–	–	–
*7	2.0	40	3.0	320	–	25.19	–	–	–
*8	2.0	40	5.0	330	–	24.93	–	–	–
9	2.0	40	1.5	94	**$7_{30-50\ nm}$**	–	–	–	–
10	2.0	40	1.5	199	**$7_{20-30\ nm}$**	–	–	–	–
11	2.0	40	1.5	161	**$15_{20-30\ nm}$**	–	–	–	–

[a]Polymerization condition; 0.0048 mmol of palladium cat, time = 30 min, 38 ml toluene (*200 ml), 2 ml CH_2Cl_2. [b]Activity: kg of product (mol Pd)$^{-1}$h^{-1}.

The reaction temperature more than 40 °C can reduce the solubility of monomer in solvent as a physical function, and as a result the activity of the catalyst would be decreased [33]. The diphenyl methyl groups block the axial position thus slowing down the potential catalyst decomposition pathways [34–36]. But the motion and rotation of aryl ring is increased at higher polymerization temperature. Therefore, perturbation occurred in coordination step through a disorder in overlap of empty d orbital of the metal center with Π-olefin orbital, leads to reduction of the activity of active centers [4]. Also, polymerization in different pressures (1.5–5 bar), at constant temperature of 40 °C, was performed (Table 1). The activity of the catalyst increased by increasing monomer pressure up to 3 bar, however, further increase of the monomer pressure to 5 bar leads to a very small increase in catalyst activity. The behavior is mainly due to higher concentration of the monomer close to the active center [37,38]. The non-linear relationship between monomer pressure and activity was previously reported [39,40]. However, higher pressure can cause reverse effect on the catalyst activity [33,41,42]. According to literature reports Pd(II) species at low ethylene pressure have beta-agostic alkyl Pd(II) and alkyl ethylene Pd(II) intermediates, at a higher ethylene pressure 5 bar, the Pd(II) species will be only the alkyl ethylene Pd(II), which would have the same activity independence of ethylene pressure[35]. All calculated densities from DSC analysis were in the range of 0.89–0.92 g/Cm^3 [43].

Table 2
Calculated parameters of Pd complex.

Parameter	Result	Parameter	Result
Pd—Cl	2.40	Pd-C_6	3.96
Pd—CH_3	2.05	CH_3—Pd—Cl	85.52
Pd—N_1	2.21	Pd—N_1—C_3	122.03
Pd—N_2	2.09	Pd—N_2—C_4	123.28
C_1=N_1	1.30	N_2—Pd—N_1	76.93
C_2=N_2	1.31	Dipole moment (Debye)	8.92
N—C_3	1.45	Band gap	0.11449
N—C_4	1.45	Total energy	−3223.34 a.u.
C_2—C_1	1.49	Charge (Mulliken)	0.005
Pd—C_5	4.28		

Selected bond distances (Ă), bonding angle (°), planes angle, dipole moment, band gap, charge, total energy of the palladium catalyst. N_1: nitrogen atom connected to the Pd atom behind Cl, N_2: nitrogen atom connected to the Pd atom behind CH_3, C_1: carbon of C—CH_3 bond in Cl side of molecular, C_2: carbon of C—CH_3 bond in CH_3 side of molecular, C_3: aryl ring carbon connected to N_1, C_4: aryl ring carbon connected to N_2, C_5: carbon atom on ortho-position of major aryl ring in Cl side of complex, C_6: carbon atom on ortho-position of major aryl ring in CH_3 side of complex.

3.3. Catalyst structure

Density functional theory (DFT) method (B3LYP as function) with LanL2DZ basis set was used to build up the structure and calculate the structural parameters of the catalyst complex. Results are depicted in Table 2 indicate optimized structures, bond distances, bond angles, dipole moments, charge and total energy of complex. The optimized structure of the complex (Fig. 1) shows the huge hindering and electronic effects of phenyl groups on ortho position which blocks axial and equatorial position of the catalyst complex. The ortho substituents retard chain transfer reactions, promote the chain walking and accelerate the rate of migratory insertion [44,45]. It has been found that there is a balance in hindering and electronic effects of the substituents on the activity and average molecular weight of the obtained polymer. To clarify, monomer diffusion, strength of the M-C bond and stability of the active center are main factor which are related to the structure and substituent, especially. Here bulky diphenyl groups in ortho position of aryl rings block the axial coordination sites which cause high stability of the active center along with a hindering effect on the monomer diffusion in equatorial position. Para substituents are characterized which have influence on the molecular weights of the polymer, branching density and the catalyst performance. The presence of ethoxy group in para position can cause an increase in activities and the average molecular weights of polyethylene [46].

3.4. Characterization of catalyst particles

The SEM images of palladium catalyst are shown in Fig. 2. It can be found that the catalyst particles are spherical in shape and multi-part with diameter of 0.92–1.15 μm. According to the morphology duplication theory the spherical catalyst particles can lead to spherical polymer particles [47]. Spherical morphology of polyethylene is important in industrial application.

3.5. Characterization of polyethylene particles

The morphology of polymers and nanocomposite were studied by SEM images. Image of polyethylene are shown in Fig. 3. It can be found that the polyethylene particles are almost spherical at both low (1.5 bar, entry 3 in Table 1) and high monomer pressure (5 bar, entry 8). The approximate size of polyethylene obtained at low pressure was 0.50–0.53 μm and for high pressure was 5.37–8.92 μm which both particle morphologies were almost similar to the catalyst particles. According to morphology replication phenomenon, spherical shape of particles increased with

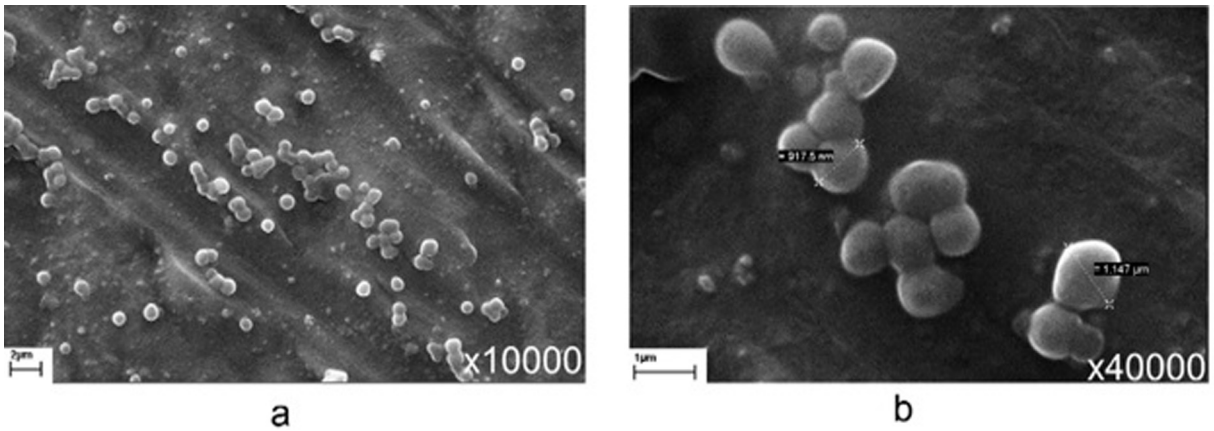

Fig. 2. SEM micrographs of Pd catalyst.

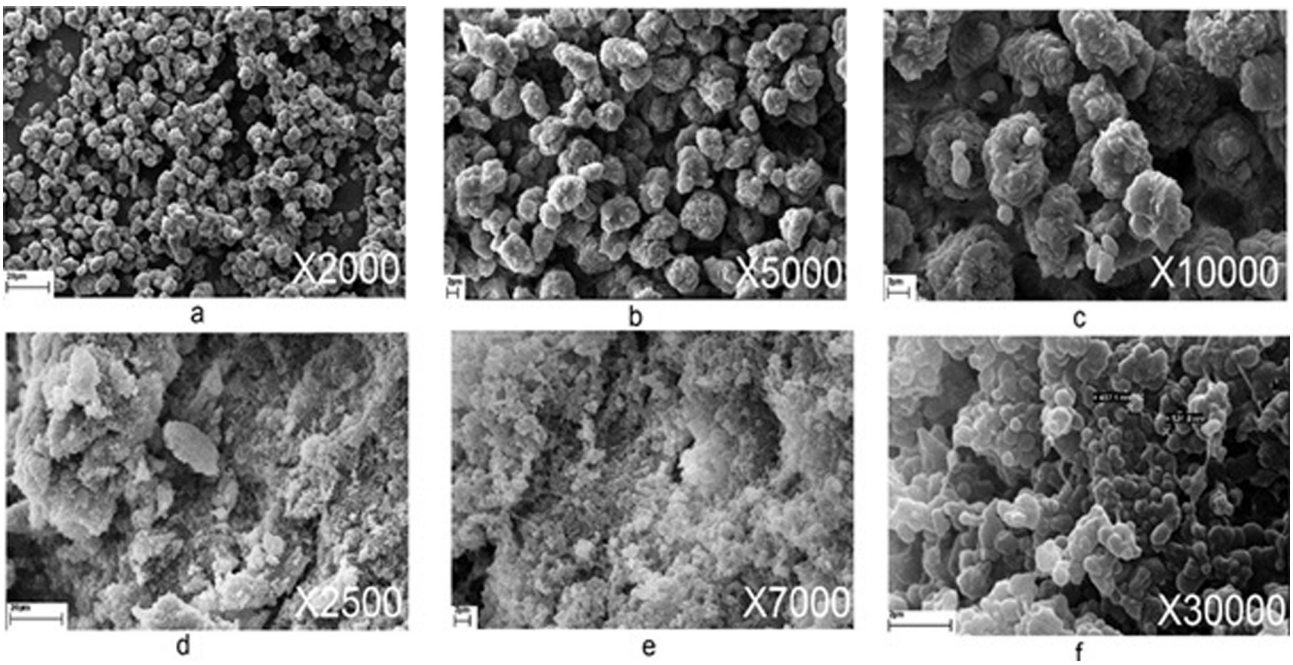

Fig. 3. SEM image of PE in different polymerization pressure (a–c) entry 8 (d–f) entry 3 of Table 1.

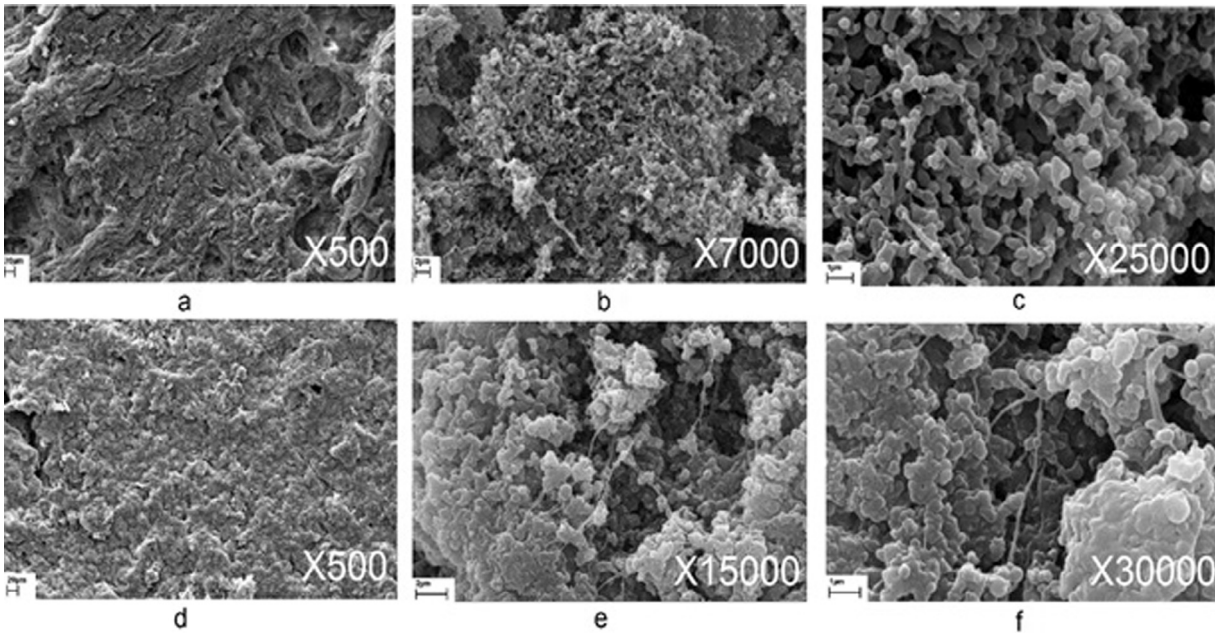

Fig. 4. SEM image of polyethylene nanocomposites (a–c) 1.46% MWCNT, (d–f) 3.88% MWCNT.

increasing of monomer pressure. The morphology of nanocomposites and presence of the MWCNT in the polymer matrix were studied by SEM (Fig. 4). The SEM images also showed the catalyst particle replication morphology into the polymer particle.

3.6. Thermal properties

DSC thermograms were recorded at second heating curves to examine the thermal behavior. The produced polymers have low melting point and broadened transition due to much high branches and weaker intermolecular forces. Moreover, the thermograms indicated that the crystallinity of PE increased from 10.5 to 23.2 with increasing polymerization temperature. The crystallinity extents were 10.5% at 40 °C (entry 3) to 16.2% and 23.2% for 60 °C (entry 5) and 80 °C (entry 6), respectively. It can be suggested that increasing kinetic energy of the monomers due to raising temperature can facilitate transfer of monomer to the catalytic active centers. It should be noted that the catalyst was stable at the high temperatures up to 80 °C. DSC thermogram of polyethylene at different polymerization pressures of monomer is depicted in Fig. 5. The crystallinity of the PE enhanced to 25.3% and 37.9% for polymerization at 3 and 5 bar monomer pressure, respectively. The

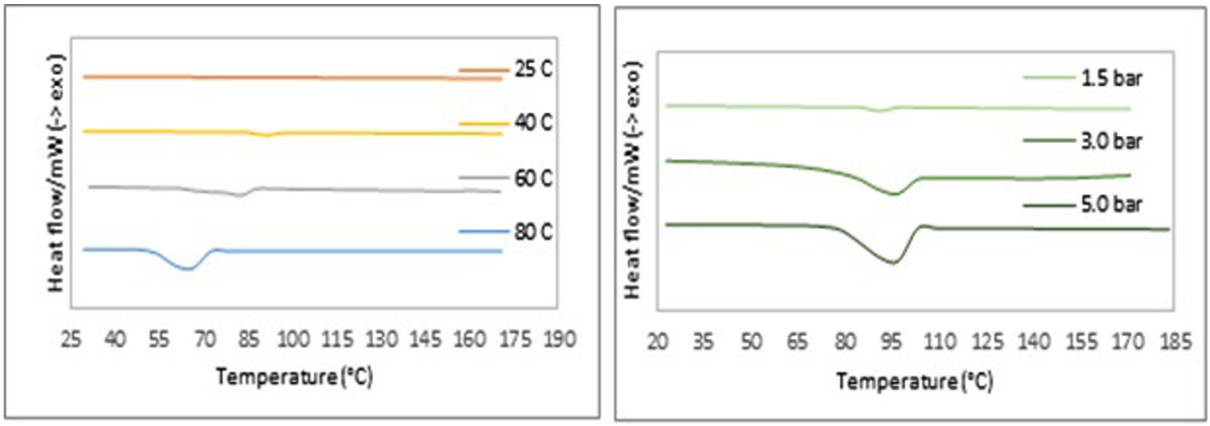

Fig. 5. DSC thermogram of produced PE, left side: In different polymerization temperature, right side: in different polymerization pressure.

observation was due to high concentration of the monomer close to the catalyst active centers which led to increasing of olefin trapping and reduction of branching extent [32].

Viscosity average molecular mass, $\bar{M}_v$ of produced PE in different pressure and temperature was in range 14300–251900 g/mol. $\bar{M}_v$ decreases with increasing polymerization temperature more than 40 °C, due to higher activation energies of chain transfer and catalyst deactivation reactions compared to chain propagation reactions [4].

Thermal stability of nanocomposite samples can be observed through the thermogravimetric and differential thermogravimetric curves (Fig. 6). The onset of degradation temperature for PE (228.3 °C) increased in the presence of 1.46% (238.0 °C) and 3.88% MWCNT (255.3 °C). Due to higher combustion temperature of nanotubes, the onset of degradation shifted to the higher temperature for nanocomposite samples. Nanotubes have a layered crystal structure and according to the fact that the crystalline structures need more heat to decomposition, so nanocomposite sample with more MWCNT showed higher thermal stability [48]. Higher amount of MWCNT caused to decreasing of catalyst activity which can be attributed to some remaining active polar functional groups on the surface of the nanocarbons that deactivated the catalyst active centers [49].

3.7. Characterization

By comparing the recorded FT-IR spectrums with references, the LDPE microstructure was confirmed which have long chain branches in structure [50]. As infrared spectrums of polymers are shown in Fig. 7, the region 1300–1400 cm^{-1} is displayed three bands assignable to CH_2 and CH_3 groups. Bands in 1377 cm^{-1} which assigned to CH_3 symmetric deformation and band in the regions of 1366 cm^{-1} and 1351 cm^{-1} belong to wagging deformation. All these samples are low-density polyethylene which prevents the molecules from packing closely together and the irregular packing cause low crystallinity content and low melting point as it was confirmed in thermal properties section [51,52].

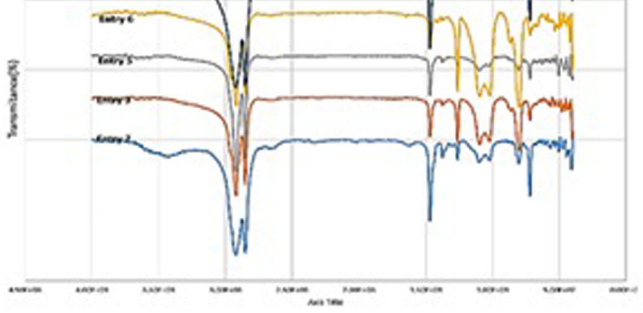

Fig. 7. Polymer FT-IR spectra.

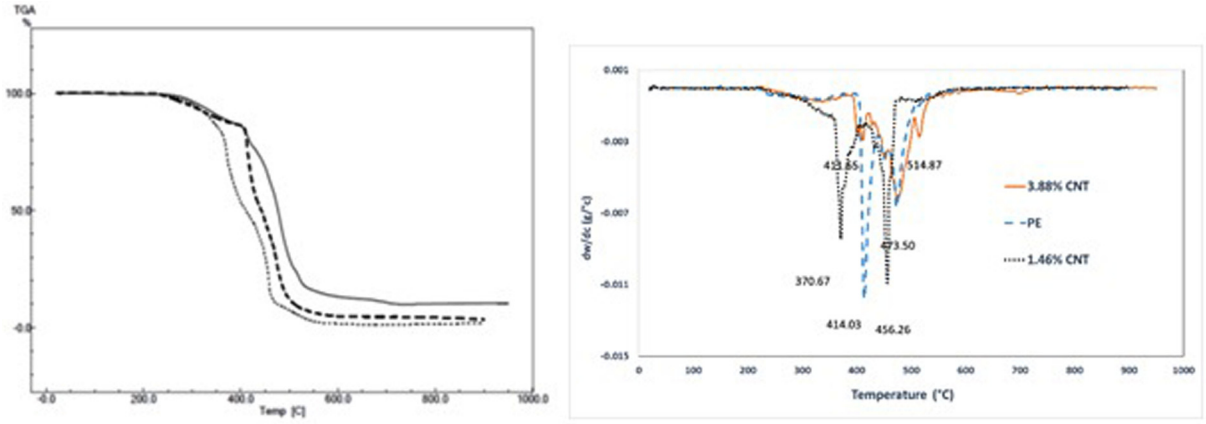

Fig. 6. Thermogravimetric and differential thermogravimetric curves of the PE and PE/nanocarbon composites synthesized through in situ polymerization (. . .. 1.46%CNT, —— PE, — 3.88%CNT).

High temperature ^{1}HNMR and ^{13}CNMR spectroscopy was used to analyze the polyethylene sample (entry 3 in Table 1). The NMR spectra were obtained at 50 °C in $CDCl_3$. The ^{13}C NMR spectra of the polymer presented in Fig. 8. The ^{13}C NMR assignments listed in Table 3 and the microstructure determination of a branched polyethylene is shown in Fig. 8. The microstructure were investigated by using ^{1}HNMR and ^{13}C NMR [53–55]. ^{1}H NMR spectroscopy is shown in Fig. 9. The ^{1}H NMR assignments listed in Table 4. It was used to determine overall branching in the polymer using the following formula [55], Results are reported in Table 1.

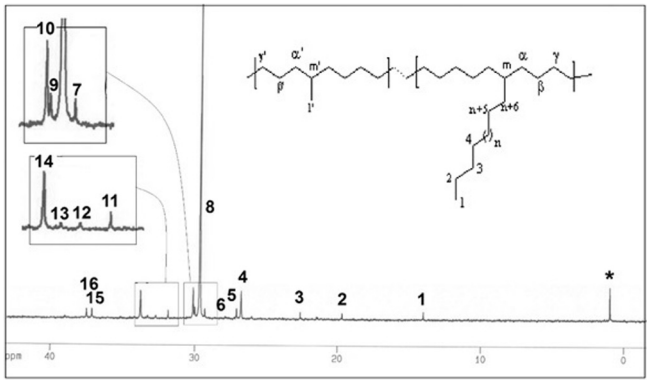

Fig. 8. ^{13}C NMR spectrum of the polymer from Table 1 entry 3 ($CDCl_3$, 50 °C), *Grease.

Table 3
^{13}C NMR assignment of polyethylene sample.

Signal	Assignment	δ(ppm)
1	$1B_n$	14.05
2	$1B_1$	19.74
3	$2B_n$	22.69
4	$(n-1)B_n$	26.81
5	βB_n	27.13
6	$\beta' B_1$	27.94
7	$4B_n$	29.37
8	$\delta\delta CH_2$	29.73
9	γB_1	30.08
10	γB_n	30.19
11	$\alpha' B_n$, $3B_n$	31.95
12	brB_1	32.84
13	$8B_n$	33.4
14	nB_n, αB_n	33.88
15	$\alpha' B_1$	37.18
16	brB_n	37.55

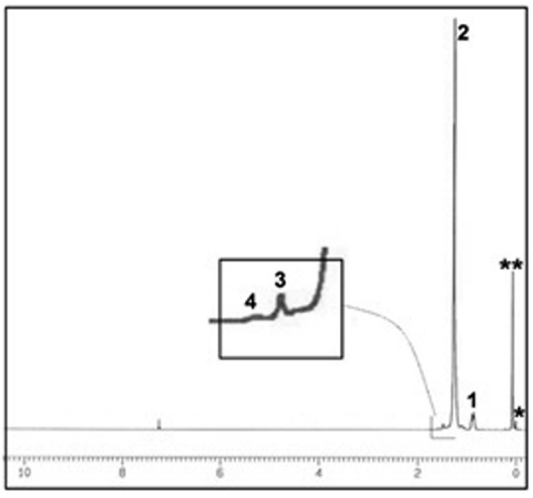

Fig. 9. ^{1}H NMR spectrum of the polymer from Table 1 entry 3 ($CDCl_3$, 50 °C). *TMS, ** grease.

Table 4
^{1}H NMR assignment of polyethylene sample.

Signal	Assignment	δ(ppm)
1	$-CH_3$	0.8
2	$(CH_2)_n$	1.27
3	—CH(L)—	1.48
4	$-CH(CH_3)-$	1.54

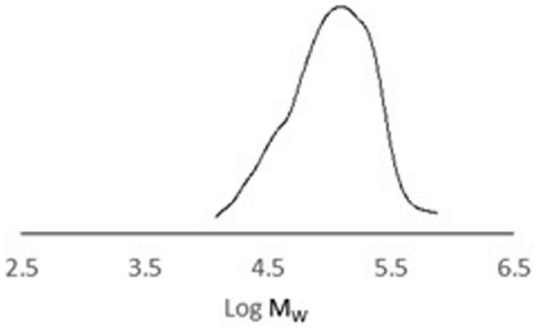

Fig. 10. GPC curve of PE (entry3).

$$\text{Branches}/1000 = \frac{CH_3\ integral}{total\ integral} \times \frac{2}{3} \times 1000 \quad (1)$$

These polymer NMR spectra confirm that chain walking α-oelfin polymerization with α-diimine Pd(II) catalyst affords polymers with methyl and long branches [8,56].

Gel permeation chromatography curve is shown in Fig. 10. Molecular weight of the polymer sample entry 3 ($\bar{M}_n = 44078$, $\bar{M}_W = 80988$) was determined by GPC in trichlorobenzene. It showed a peak along with a shoulder which can attribute to difference molecular weight of polymer chains, with almost narrow molecular weight distribution and polydispersity index (PDI) 1.83.

4. Conclusion

The prepared palladium (II) α-diimine catalyst with benzhydryl-derived ligand framework and ethoxy group in the para position of *N*-aryl group was an active catalyst in ethylene polymerization. The effects of parameters such as polymerization temperature, co-catalyst to catalyst ratio and monomer pressure were investigated. The optimum activity of the catalyst was obtained at 40 °C in 5 atm ethylene pressure in presence of 2 equivalent co-catalyst. Study of the properties of the resulting polymeric products showed that the increasing in monomer pressure led to polyethylenes with higher molecular weight, melting point and crystallinity. The diphenyl methyl groups block the axial position very well and retard catalyst decomposition. This α-Diimine catalyst was examined for temperature ethylene polymerization. The experiments indicated that the catalyst is active up to 80 °C which produced polyethylene with branching density of 40.5/1000C and melting point in the range of 66–111 °C. These features were higher than amounts reported by Chen group for similar catalyst bearing Me, OMe, Cl and CF_3 groups. ^{13}C NMR, ^{1}H NMR of PE confirmed the synthesis of PE with long branches and moderate branching density. The ligand electronic effects controlled by

ethoxy group as an electron-donating group and it led to increase the thermal stability of catalyst and polymer branching density. Also the melting point of produced polymer is influenced by the ligand electronic effect. GPC analysis resulted a peak along with a little shoulder which attributed to difference molecular weight of polymer chains with almost narrow molecular weight distribution (PDI = 1.83). Also in this report MWCNT was used for nanocomposite preparation. TGA and DTA curves indicated that increasing MWCNT percentage up to 3.88%, enhance thermal stability up to 255.34 °C. Spherical morphologies of catalyst particles, polymers and nanocomposites were investigated by SEM images and confirmed replication phenomena.

Acknowledgements

The authors are grateful of Ferdowsi university of Mashhad (FUM) and Shahrood University of Technology for all their cooperations. Also we would like to thank Dr Navid Ramezanian and Mr Mostafa Khoshsefat for their cooperation.

Appendix A. Supplementary data

Supplementary data associated with this article can be found, in the online version, at http://dx.doi.org/10.1016/j.ica.2017.05.005. These data include MOL file of palladium complex described in this article.

References

[1] S. Damavandi, N. Samadieh, S. Ahmadjo, Z. Etemadinia, G.H. Zohuri, Novel Ni-based FI catalyst for ethylene polymerization, Eur. Polym. J. 64 (2015) 118–125.
[2] H. Hu, L. Zhang, H. Gao, F. Zhu, Q. Wu, Design of thermally stable amine-imine nickel catalyst precursors for living polymerization of ethylene: effect of ligand substituents on catalytic behavior and polymer properties, Chemistry 20 (11) (2014) 3225–3233.
[3] L. Guo, S. Dai, C. Chen, Investigations of the ligand electronic effects on α-diimine nickel (II) catalyzed ethylene polymerization, Polymers 8 (2) (2016) 37.
[4] D.P. Gates, S.A. Svejda, E. Oñate, C.M. Killian, L.K. Johnson, P.S. White, M. Brookhart, Synthesis of branched polyethylene using (α-diimine) nickel (II) catalysts: influence of temperature, ethylene pressure, and ligand structure on polymer properties, Macromolecules 33 (7) (2000) 2320–2334.
[5] S. Mecking, Olefin polymerization by late transition metal complexes—a root of Ziegler catalysts gains new ground, Angew. Chem. Int. Ed. 40 (3) (2001) 534–540.
[6] E. Yue, Q. Xing, L. Zhang, Q. Shi, X.-P. Cao, L. Wang, C. Redshaw, W.-H. Sun, Synthesis and characterization of 2-(2-benzhydrylnaphthyliminomethyl) pyridylnickel halides: formation of branched polyethylene, Dalton Trans. 43 (8) (2014) 3339–3346.
[7] L. Fan, S. Du, C.Y. Guo, X. Hao, W.H. Sun, 1-(2, 6-dibenzhydryl-4-fluorophenylimino)-2-aryliminoacenaphthylylnickel halides highly polymerizing ethylene for the polyethylenes with high branches and molecular weights, J. Polym. Sci., Part A: Polym. Chem. 53 (11) (2015) 1369–1378.
[8] S. Dai, X. Sui, C. Chen, Highly robust palladium (II) α-diimine catalysts for slow-chain-walking polymerization of ethylene and copolymerization with methyl acrylate, Angew. Chem. Int. Ed. 54 (34) (2015) 9948–9953.
[9] J.L. Rhinehart, L.A. Brown, B.K. Long, A robust Ni (II) α-diimine catalyst for high temperature ethylene polymerization, J. Am. Chem. Soc. 135 (44) (2013) 16316–16319.
[10] J.L. Rhinehart, N.E. Mitchell, B.K. Long, Enhancing α-diimine catalysts for high-temperature ethylene polymerization, ACS Catal. 4 (8) (2014) 2501–2504.
[11] S.S. Ivanchev, A.V. Yakimansky, D.G. Rogozin, Quantum-chemical calculations of the effect of cycloaliphatic groups in α-diimine and bis (imino) pyridine ethylene polymerization precatalysts on their stabilities with respect to deactivation reactions, Polymer 45 (19) (2004) 6453–6459.
[12] K.R. Kumar, S. Sivaram, Ethylene polymerization using iron (II) bis (imino) pyridyl and nickel (diimine) catalysts: effect of cocatalysts and reaction parameters, Macromol. Chem. Phys. 201 (13) (2000) 1513–1520.
[13] T.M. Smit, A.K. Tomov, V.C. Gibson, A.J. White, D.J. Williams, Dramatic effect of heteroatom backbone substituents on the ethylene polymerization behavior of bis (imino) pyridine iron catalysts, Inorg. Chem. 43 (21) (2004) 6511–6512.
[14] I. Kim, B.H. Han, Y.-S. Ha, C.-S. Ha, D.-W. Park, Effect of substituent position on the ethylene polymerization by Fe (II) and Co (II) pyridyl bis-imine catalysts, Catal. Today 93 (2004) 281–285.
[15] S. Dai, S. Zhou, W. Zhang, C. Chen, Systematic investigations of ligand steric effects on α-diimine palladium catalyzed olefin polymerization and copolymerization, Macromolecules (2016).
[16] J.A. Kim, D.G. Seong, T.J. Kang, J.R. Youn, Effects of surface modification on rheological and mechanical properties of CNT/epoxy composites, Carbon 44 (10) (2006) 1898–1905.
[17] Y. Zou, Y. Feng, L. Wang, X. Liu, Processing and properties of MWNT/HDPE composites, Carbon 42 (2) (2004) 271–277.
[18] Y. Xue, W. Wu, O. Jacobs, B. Schädel, Tribological behaviour of UHMWPE/HDPE blends reinforced with multi-wall carbon nanotubes, Polym. Testing 25 (2) (2006) 221–229.
[19] T. Chang, L.R. Jensen, A. Kisliuk, R. Pipes, R. Pyrz, A. Sokolov, Microscopic mechanism of reinforcement in single-wall carbon nanotube/polypropylene nanocomposite, Polymer 46 (2) (2005) 439–444.
[20] Z. Yaping, Z. Aibo, C. Qinghua, Z. Jiaoxia, N. Rongchang, Functionalized effect on carbon nanotube/epoxy nano-composites, Mater. Sci. Eng. A 435 (2006) 145–149.
[21] K.P. Ryan, M. Cadek, V. Nicolosi, D. Blond, M. Ruether, G. Armstrong, H. Swan, A. Fonseca, J.B. Nagy, W.K. Maser, Carbon nanotubes for reinforcement of plastics? A case study with poly(vinyl alcohol), Compos. Sci. Technol. 67 (7) (2007) 1640–1649.
[22] A.R. Bhattacharyya, T. Sreekumar, T. Liu, S. Kumar, L.M. Ericson, R.H. Hauge, R. E. Smalley, Crystallization and orientation studies in polypropylene/single wall carbon nanotube composite, Polymer 44 (8) (2003) 2373–2377.
[23] Z. Wang, M. Lu, H.-L. Li, X.-Y. Guo, SWNTs–polystyrene composites preparations and electrical properties research, Mater. Chem. Phys. 100 (1) (2006) 77–81.
[24] J. Xiong, Z. Zheng, X. Qin, M. Li, H. Li, X. Wang, The thermal and mechanical properties of a polyurethane/multi-walled carbon nanotube composite, Carbon 44 (13) (2006) 2701–2707.
[25] K. Ryan, M. Cadek, V. Nicolosi, S. Walker, M. Ruether, A. Fonseca, J. Nagy, W. Blau, J. Coleman, Multiwalled carbon nanotube nucleated crystallization and reinforcement in poly (vinyl alcohol) composites, Synth. Met. 156 (2) (2006) 332–335.
[26] L. Qu, Y. Lin, D.E. Hill, B. Zhou, W. Wang, X. Sun, A. Kitaygorodskiy, M. Suarez, J. W. Connell, L.F. Allard, Polyimide-functionalized carbon nanotubes: synthesis and dispersion in nanocomposite films, Macromolecules 37 (16) (2004) 6055–6060.
[27] S. Ruan, P. Gao, X.G. Yang, T. Yu, Toughening high performance ultrahigh molecular weight polyethylene using multiwalled carbon nanotubes, Polymer 44 (19) (2003) 5643–5654.
[28] M. Abdel-Goad, P. Pötschke, Rheological characterization of melt processed polycarbonate-multiwalled carbon nanotube composites, J. Nonnewton. Fluid Mech. 128 (1) (2005) 2–6.
[29] Q. Zhang, S. Rastogi, D. Chen, D. Lippits, P.J. Lemstra, Low percolation threshold in single-walled carbon nanotube/high density polyethylene composites prepared by melt processing technique, Carbon 44 (4) (2006) 778–785.
[30] T. McNally, P. Pötschke, P. Halley, M. Murphy, D. Martin, S.E. Bell, G.P. Brennan, D. Bein, P. Lemoine, J.P. Quinn, Polyethylene multiwalled carbon nanotube composites, Polymer 46 (19) (2005) 8222–8232.
[31] M. Khoshsefat, S. Ahmadjo, S. Mortazavi, G. Zohuri, Reinforcement effects of nanocarbons on catalyst behaviour and polyethylene properties through in situ polymerization, RSC Adv. 6 (91) (2016) 88625–88632.
[32] H. Zohuri, Hamid Pourtaghi-Zahed, Polym. Bull 70 (2013) 1769–1780.
[33] H. Jiang, J. Lu, F. Wang, Polymerization of ethylene using a nickel α-diimine complex covalently supported on SiO_2–$MgCl_2$ bisupport, Polym. Bull. 65 (8) (2010) 767–777.
[34] A. Berkefeld, S. Mecking, Deactivation pathways of neutral Ni (II) polymerization catalysts, J. Am. Chem. Soc. 131 (4) (2009) 1565–1574.
[35] D.J. Tempel, L.K. Johnson, R.L. Huff, P.S. White, M. Brookhart, Mechanistic studies of Pd (II)–α-diimine-catalyzed olefin polymerizations, J. Am. Chem. Soc. 122 (28) (2000) 6686–6700.
[36] L. Guo, H. Gao, Q. Guan, H. Hu, J. Deng, J. Liu, F. Liu, Q. Wu, Substituent effects of the backbone in α-diimine palladium catalysts on homo-and copolymerization of ethylene with methyl acrylate, Organometallics 31 (17) (2012) 6054–6062.
[37] F. AlObaidi, Z. Ye, S. Zhu, Ethylene polymerization with homogeneous nickel–diimine catalysts: effects of catalyst structure and polymerization conditions on catalyst activity and polymer properties, Polymer 45 (20) (2004) 6823–6829.
[38] L. Guo, S. Dai, X. Sui, C. Chen, Palladium and nickel catalyzed chain walking olefin polymerization and copolymerization, ACS Catal. 6 (1) (2015) 428–441.
[39] M. Khoshsefat, G.H. Zohuri, N. Ramezanian, S. Ahmadjo, M. Haghpanah, Polymerization of ethylene using a series of binuclear and a mononuclear Ni (II)-based catalysts, J. Polym. Sci., Part A: Polym. Chem. 54 (18) (2016) 3000–3011.
[40] H. Arabi, M. Beheshti, M. Yousefi, N.G. Hamedani, M. Ghafelebashi, Study of triisobutylaluminum as cocatalyst and processing parameters on ethylene polymerization performance of α-diimine nickel (II) complex by response surface method, Polym. Bull. 70 (10) (2013) 2765–2781.
[41] L.C. Simon, C.P. Williams, J.B. Soares, R.F. de Souza, Kinetic investigation of ethylene polymerization catalyzed by nickel-diimine catalysts, J. Mol. Catal. A: Chem. 165 (1) (2001) 55–66.
[42] M.D. Leatherman, S.A. Svejda, L.K. Johnson, M. Brookhart, Mechanistic studies of nickel (II) alkyl agostic cations and alkyl ethylene complexes: investigations of chain propagation and isomerization in (α-diimine) Ni (II)-catalyzed ethylene polymerization, J. Am. Chem. Soc. 125 (10) (2003) 3068–3081.

[43] C. Carlini, A. D'Alessio, S. Giaiacopi, R. Po, M. Pracella, A.M.R. Galletti, G. Sbrana, Linear low-density polyethylenes by co-polymerization of ethylene with 1-hexene in the presence of titanium precursors and organoaluminium co-catalysts, Polymer 48 (5) (2007) 1185–1192.
[44] J. Liu, Y. Li, Y. Li, N. Hu, Ethylene polymerization by (α-diimine) nickel (II) complexes bearing different substituents on para-position of imines activated with MMAO, J. Appl. Polym. Sci. 109 (2) (2008) 700–707.
[45] J. Merna, Z. Hošťálek, J. Peleška, J. Roda, Living/controlled olefin polymerization initiated by nickel diimine complexes: the effect of ligand ortho substituent bulkiness, Polymer 50 (21) (2009) 5016–5023.
[46] C.S. Popeney, Z. Guan, Effect of ligand electronics on the stability and chain transfer rates of substituted Pd (II) α-diimine catalysts (1), Macromolecules 43 (9) (2010) 4091–4097.
[47] Q.-G. Huang, Z. Liu, W.-J. Liu, J.-J. Yi, X.-L. Zhang, K.-J. Gao, H.-B. Huang, W. Liu, H.-P. Zhen, W.-T. Yang, Preparation and self-assembly of global nano-particles of $MgCl_2$-CH_3CH_2OH complex, Acta Polym. Sin. 8 (2012) 883–886.
[48] B. Singh, P. Saini, T. Gupta, P. Garg, G. Kumar, I. Pande, S. Pande, R. Seth, S. Dhawan, R. Mathur, Designing of multiwalled carbon nanotubes reinforced low density polyethylene nanocomposites for suppression of electromagnetic radiation, J. Nanopart. Res. 13 (12) (2011) 7065–7074.
[49] M.A. Milani, D. González, R. Quijada, N.R. Basso, M.L. Cerrada, D.S. Azambuja, G. B. Galland, Polypropylene/graphene nanosheet nanocomposites by in situ polymerization: Synthesis, characterization and fundamental properties, Compos. Sci. Technol. 84 (2013) 1–7.
[50] J. Gulmine, P. Janissek, H. Heise, L. Akcelrud, Polyethylene characterization by FTIR, Polym. Testing 21 (5) (2002) 557–563.
[51] A.A. Klyosov, Wood-Plastic Composites, John Wiley & Sons, 2007.
[52] C. Vasile, M. Pascu, Practical guide to polyethylene, iSmithers Rapra Publishing, 2005.
[53] G.B. Galland, R.F. de Souza, R.S. Mauler, F.F. Nunes, ^{13}C NMR Determination of the composition of linear low-density polyethylene obtained with [η3-methallyl-nickel-diimine] PF6 complex, Macromolecules 32 (5) (1999) 1620–1625.
[54] G.B. Galland, R. Quijada, R. Rojas, G. Bazan, Z.J. Komon, NMR study of branched polyethylenes obtained with combined Fe and Zr catalysts, Macromolecules 35 (2) (2002) 339–345.
[55] A.C. Gottfried, M. Brookhart, Living and block copolymerization of ethylene and α-olefins using palladium (II)-α-diimine catalysts, Macromolecules 36 (9) (2003) 3085–3100.
[56] L. Guo, S. Dai, X. Sui, C. Chen, Palladium and nickel catalyzed chain walking olefin polymerization and copolymerization, ACS Catal. 6 (2016) 428–441.